THE JOURNAL OF PHYSICAL CHEMISTRY LETTERS
A JOURNAL OF THE AMERICAN CHEMICAL SOCIETY

pubs.acs.org/JPCL

Letter

Fabrication of Addressable Perovskite Film Arrays for High-Performance Photodetection and Real-Time Image Sensing Application

Bin Wang, Chao Zhang, Bin Zeng, Chun-Yan Wu,* Chao Xie, Di Wu, Yu-Xue Zhou, and Lin-Bao Luo*

Cite This: *J. Phys. Chem. Lett.* 2021, 12, 2930−2936

Read Online

ACCESS | Metrics & More | Article Recommendations | Supporting Information

ABSTRACT: Patterned growth of periodic perovskite film arrays is essential for application in sensing devices and integrated optoelectronic systems. Herein, we report on patterned growth of addressable perovskite photodetector arrays through an uncured polydimethylsiloxane (PDMS) oligomer-assisted solution-processed approach, in which a periodic hydrophilic/hydrophobic substrate replicating the predesigned patterns of the PDMS stamp was formed due to the migration of uncured siloxane oligomers in the PDMS stamp to the intimately contacted substrate. By using this technique, $MAPbI_3$ film photodetector arrays with neglectable pixel-to-pixel variation, a responsivity of 2.83 A W^{-1}, specific detectivity of 5.4 × 10^{12} Jones, and fast response speed of 52.7/57.1 μs (response/recovery time) were achieved. An 8 × 8 addressable photodetector array was further fabricated, which functioned well as a real-time image sensor with reasonable spatial resolution. It is believed that the proposed strategy will find potential application in large-scale fabrication of other photodetector arrays, which might be potentially important for future integrated optoelectronic devices.

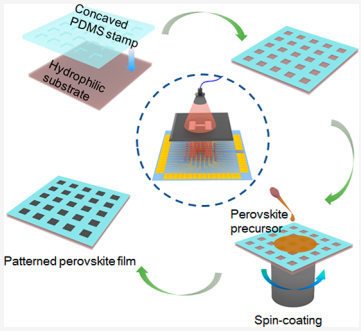

Downloaded via HEFEI UNIV OF TECHNOLOGY on August 4, 2021 at 01:06:50 (UTC).
See https://pubs.acs.org/sharingguidelines for options on how to legitimately share published articles.

Photodetectors are significant due to their potential applications in fields such as optical communication, high-density optical information technology, chemical and biological imaging/sensing, night vision and safety monitoring, etc.[1−3] Among the great variety of photosensitive semiconductor materials, metal halide perovskites (MHPs) stand out due to their superior physical and optoelectronic properties.[4−6] To date, various perovskite materials in the form of bulk polycrystalline films, single crystals, and low-dimensional nanostructures have been intensively studied and tremendous efforts have been focused on the development of high-efficiency photodetectors.[7−10] More importantly, practical device application of perovskites in integrated optoelectronic devices such as artificial eyes, electronic skin, camera modules, and digital displays has led to an increasing demand for optoelectronic device arrays.[11−13] The conventional photolithography process cannot be directly applied to the patterning of perovskite materials due to the solubility of perovskites in commonly used solvents and the sensitivity of the organic component to moisture.[14,15] Until now, a variety of technologies have been developed for the nondestructive patterning of perovskite arrays with precisely controlled shapes and positions.[16−25] However, despite the exciting progress, expensive apparatuses, complex templates, or high-quality and continuous hydrophobic layers are normally required, which makes the fabrication process time-consuming and costly. A facile and cost-efficient strategy for the patterned growth of perovskite arrays is still urgently required.

PDMS has been widely used for soft lithographic patterning due to its high hydrophobicity as well as good thermal and oxidative stability. For example, well-aligned perovskite nanowire arrays can be obtained by polydimethylsiloxane (PDMS) template-assisted geometrically confined growth[26] and nanoimprinting technology.[14] Highly ordered full-color light-emitting diodes with ultrafine pixels can be conformally integrated by microcontact printing (μ-CP)[27] and intaglio transfer printing processes using PDMS as a stamp.[28] Notably, unexpected "contaminant" PDMS material is known to remain on the substrate, leaving an unfavorable hydrophobic surface. The contaminant is believed to be the small uncured siloxane oligomers in PDMS migrating from the inner-space to the free-surface and then to the substrate as a result of the concentration gradient.[29] Herein, inspired by this, we propose an uncured PDMS oligomer assisted patterned growth of perovskite film arrays by using a predesigned PDMS stamp. With this technique, $MAPbI_3$ perovskite film arrays have been obtained, which present decent photoresponse characteristics with the responsivity (R), specific detectivity (D^*), and response speed of 2.83 A W^{-1}, 5.4 × 10^{12} Jones, and 52.7/57.1 μs (response/recovery time), with satisfactory uniformity.

Received: February 16, 2021
Accepted: March 10, 2021
Published: March 16, 2021

© 2021 American Chemical Society

https://doi.org/10.1021/acs.jpclett.1c00521
J. Phys. Chem. Lett. 2021, 12, 2930−2936

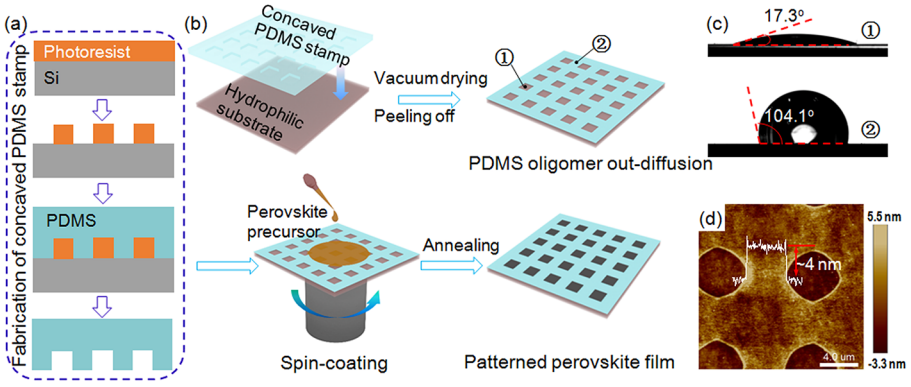

Figure 1. (a) Schematic illustration for fabricating the concaved PDMS stamp. (b) Schematic illustration of the process for patterned growth of perovskite film arrays. (c) Contact angles of the perovskite precursor solution on the substrate regions without (top panel) and with (bottom panel) uncured PDMS oligomers, respectively. (d) AFM image of the patterned substrate with uncured PDMS oligomer molecules.

Furthermore, an 8 × 8 addressable perovskite photodetector arrays without crosstalk has been fabricated. With the assistance of a customized data acquisition system, the photodetector arrays can function as a real-time visible light image sensor with reasonable spatial resolution. This work suggests that the addressable photodetector arrays derived from the present synthetic method may find application in the field of integrated optoelectronic devices.

PDMS stamps with predesired patterns were fabricated through UV photolithography and replica molding schematically shown in Figure 1a (please refer to the Supporting Information for details).[30] The as-prepared PDMS stamp was gently placed face down on the surface of the precleaned substrate, which was then put in a vacuum drying oven with the chamber pressure set to be 0.03 MPa and kept at room temperature for about 4 h (Figure 1b). Figure 1c shows the contact angles of the perovskite precursor solution on different regions of the substrate after peeling off the PDMS stamp. Clearly, region ① that has not been contacted with the PDMS stamp shows a small contact angle of 17.3°, verifying the good hydrophilicity of the substrate. Region ② shows a larger contact angle of 104.1°, suggesting the formation of a hydrophobic layer in the region. We believe that the hydrophobic layer consists of the uncured PDMS oligomers that migrate to the substrate from the PDMS stamp.[29] Further atomic force microscopy (AFM) imaging reveals that the thickness of the uncured PDMS oligomers on the substrate is about 4 nm (Figure 1d). During the process of spin-coating, the hydrophilic region would be wetted by the perovskite precursor solution while the excess solution on the hydrophobic region would be removed from the substrate by the centrifugal force due to the dewetting property. A perovskite film with desired micropatterns would then be formed on the substrate after thermal annealing (please refer to the Supporting Information for details).

Figure 2a displays the SEM images of the perovskite films with periodic square arrays, and the corresponding XRD pattern (Figure 2b) is consistent with a previously reported $MAPbI_3$ film.[31] Apparently, the obtained films possess a regular and uniform shape with sharp edges. No obvious pinholes and cracks can be observed, verifying the selective growth on the substrate. The magnified SEM image (Figure 2a inset) further presents a compact and uniform surface, implying the homogeneous growth of the perovskite within the hydrophilic region. In addition to square array, $MAPbI_3$ perovskite film

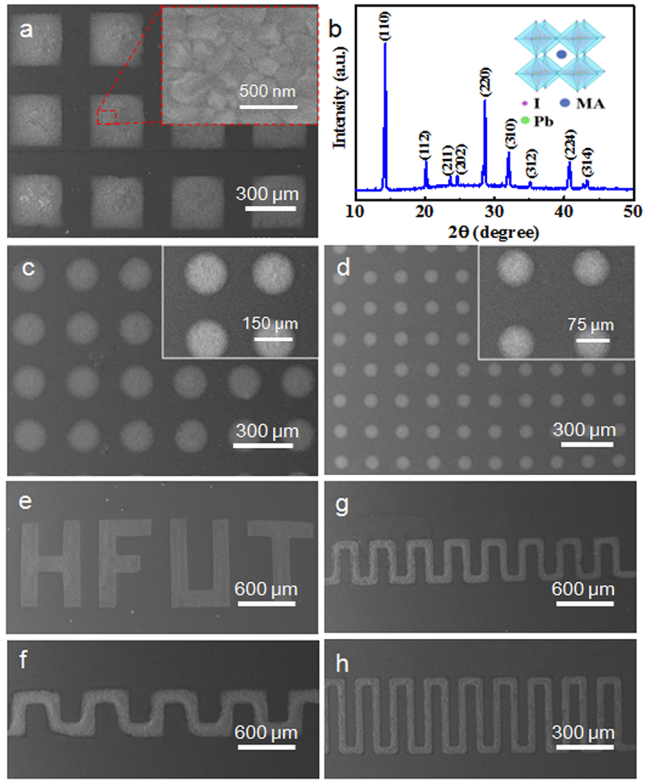

Figure 2. (a) SEM images and (b) XRD pattern of the perovskite films with the patterns of periodic square arrays. (a inset) Magnified SEM image. SEM images of the perovskite films with the patterns of periodic circular arrays with diameters of (c) 150 and (d) 75 μm, respectively. SEM images of the perovskite films arranged in (e) a HFUT pattern and a meandering line with widths of (f) 100, (g) 50, and (h) 25 μm, respectively.

arrays with other morphologies and different diameters can also been easily obtained (Figure 2c, d). Interestingly, the proposed process has also been applied to prepare perovskite films arranged in other complex micropatterns, including "HFUT" characters and meandering lines with widths of 100, 50, and 25 μm, respectively (Figure 2e–h). Specifically, even for the line width and space width of only 25 μm, a continuous line of perovskite film with clear edges can still be realized.

Apart from the SiO_2/Si substrate, the patterned growth of $MAPbI_3$ perovskite film arrays can also be realized on other substrates including SiO_2/Si, FTO, ITO, and flexible

https://doi.org/10.1021/acs.jpclett.1c00521
J. Phys. Chem. Lett. 2021, 12, 2930−2936

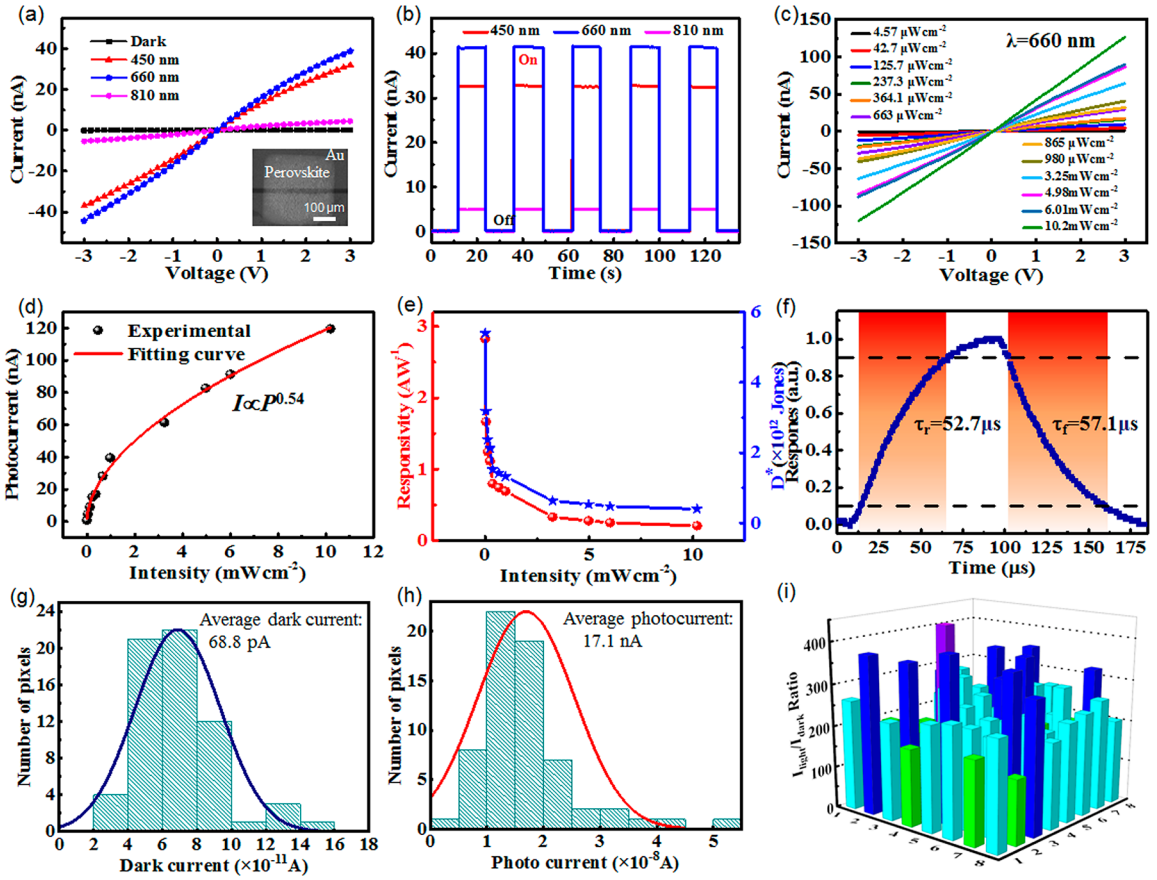

Figure 3. (a) Current (I)−voltage (V) curves and (b) time-dependent photoresponse of the $MAPbI_3$ film based photodetector upon illumination with different wavelengths at a fixed power density of 1.02 mW cm^{-2}. (a inset) Typical optical photograph of the photodetector. (c) $I-V$ curves upon 660 nm illumination with varied light intensities. (d) Photocurrent as a function of incident light intensity at 3 V bias voltage. (e) Responsivity and specific detectivity as a function of light intensity. (f) Single magnified photoresponse curve at the frequency of 6 kHz to calculate the response time. Distribution of the channel current for the perovskite photodetector arrays (g) in the dark and (h) upon homogeneous white light illumination light (1.25 mW cm^{-2}) under 3 V bias voltage. (i) 3D diagram showing the I_{light}/I_{dark} ratio for each pixel device.

fluorophlogopite mica [$KMg_3(AlSi_3O_{10})F_2$]. SEM images (Figure S4) show that well-patterned squares with sharp edges and uniform morphologies have been obtained. This verifies the compatibility of PDMS stamps with various substrates, and we believe that it may be ascribed to the good flexibility of PDMS. Unlike a conventional hard template, the PDMS stamp has a high tolerance with the substrate as well as the surface roughness. Intimate contact can be formed between the PDMS stamp and the substrates. With the migrating of the uncured siloxane oligomers, a uniform hydrophobic layer can be formed in the intimately contacted region while the uncontacted region remains hydrophilic. Further study also finds that this growth process can actually be used to grow other perovskite materials, such as Cs doped $FAPbI_3$ perovskite film arrays and $MAPbI_{3-x}Cl_x$ perovskite film arrays. As shown in Figures S5 and S6, both materials show the well-defined square patterns and remarkable photoresponse. Therefore, the proposed PDMS oligomer-assisted patterned growth method provides a facial and versatile strategy for the solution-based fabrication of perovskite film arrays, which holds great potential for application in integrated optoelectronic devices as well as wearable optoelectronic devices.

For optoelectronic characterization, 50 nm parallel Au electrode arrays with 20 μm channel length were deposited onto the as-obtained $MAPbI_3$ perovskite film arrays through a shadow mask. The SEM image of a representative pixel device (inset in Figure 3a) shows that a continuous and compact perovskite film was obtained across the device channel. Figure 3a plots the current−voltage ($I-V$) curves of the pixel device in the dark and upon illumination with different wavelengths. It can be observed that the photocurrent depends almost linearly on the applied voltage. At a bias voltage of 3 V, the device displayed a low dark current of about 52 pA. When illuminated by visible light (450 and 660 nm) and NIR light (810 nm) at a fixed power density of 1.02 mW cm^{-2}, the channel current increased remarkably to about 32, 39, and 4.4 nA, respectively, revealing a high-performance photoresponse of the device to incident illumination. What is more, the device exhibits a higher sensitivity to visible light (450 and 660 nm) than NIR light (810 nm), which is consistent with previously reported photoresponse of the $MAPbI_3$ perovskite film.[32] Time-dependent photoresponse of the device was also measured at 3 V bias voltage. As displayed in Figure 3b, the device can be readily switched between on- and off-states upon illumination of periodically switched incident light, showing good stability and reproducibility. The I_{light}/I_{dark} ratio was up to 1.09×10^2 at 810 nm illumination, suggesting potential as a high-performance visible−NIR photodetector.

The photoresponse of the device shows a strong dependence on the intensity of the incident light. As illustrated in Figure 3c, the channel current increases monotonously from 0.83 to 119.1 nA with increasing light intensity from 4.57 μW cm^{-2} to

https://doi.org/10.1021/acs.jpclett.1c00521
J. Phys. Chem. Lett. 2021, 12, 2930−2936

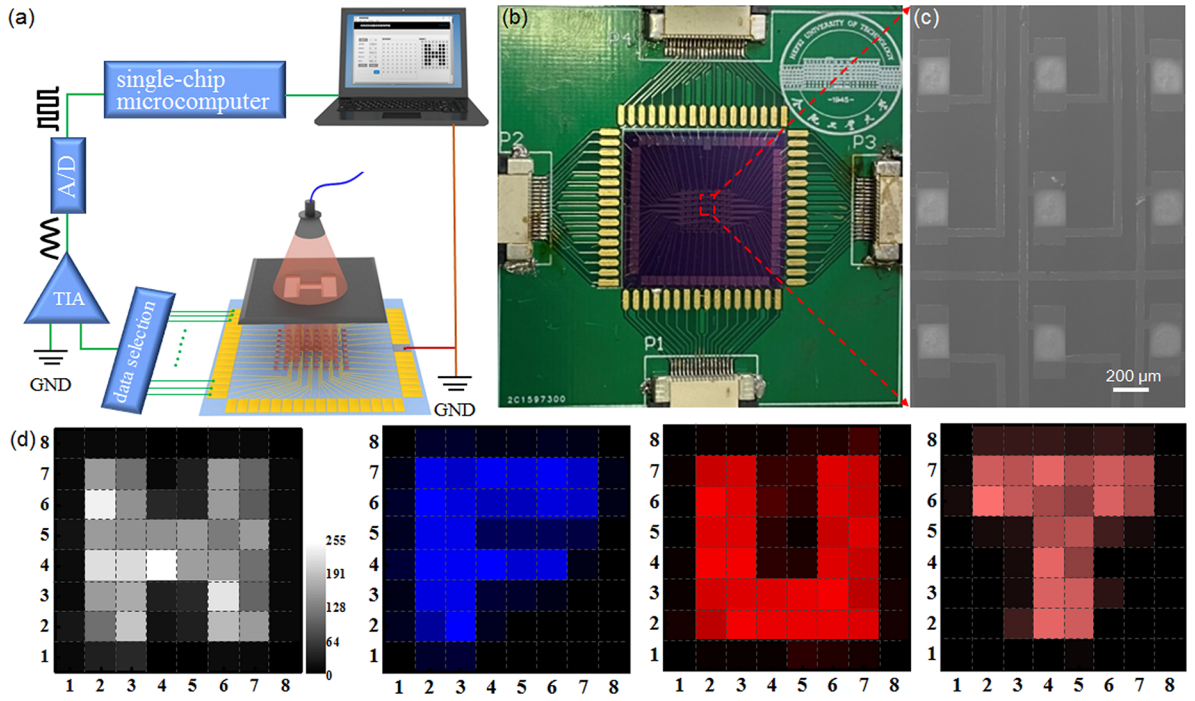

Figure 4. (a) Schematic illustration of the customized data acquisition system for real-time imaging. (b) Photograph of the addressable 8 × 8 perovskite photodetector arrays mounted on a printed circuit board. (c) SEM image of the pixels marked by the red dotted square in b. (d) Letters "H", "F", "U", and "T" displayed on the screen when the photodetector arrays are illuminated with white light (1.25 mW cm^{-2}), blue light (450 nm, 12.7 mW cm^{-2}), red light (660 nm, 10.1 mW cm^{-2}), and near-infrared light (810 nm, 9.51 mW cm^{-2}), respectively.

10.2 mW cm^{-2} at 3 V bias voltage. This may be ascribed to the increased photogenerated electron−hole pairs when illuminated by the incident with stronger light intensity. The photocurrent curve as a function of light intensity was further fitted to be $I \propto P^{0.54}$ over the wide light intensity range (Figure 3d). The noninteger exponent θ suggests the existence of recombination loss in the device, which may arise from the carrier recombination occurred at the grain boundaries and surface trap states in the perovskite film.[33]

To quantitatively assess the performance of the present perovskite photodetector, key performance parameters, including responsivity (R), specific detectivity (D^*), and external quantum efficiency (EQE), were calculated according to the following equations[34,35]

$$R = \frac{I_{light} - I_{dark}}{P_{in}S} = \mathrm{EQE}\left(\frac{e\lambda}{hc}\right) \quad (1)$$

$$D^* = \frac{RS^{1/2}}{(2eI_{dark})^{1/2}} \quad (2)$$

where I_{light}, I_{dark}, P_{in}, S, e, λ, h, and c represent the channel current upon illumination, dark current, incident light intensity, the effective illuminating area (300 μm × 20 μm for this device), the elementary electronic charge (1.6 × 10^{-19} C), the incident light wavelength, Planck's constant, and the speed of light, respectively. As plotted in Figure 3e, R and D^* decrease with the increase of the incident light intensity and reach 2.83 A W^{-1} and 5.4 × 10^{12} Jones upon 660 nm illumination with the lower light intensity of 4.57 μW cm^{-2}, respectively, which are slightly smaller than those of the devices based on $MAPbI_3$ single crystals[36] and aligned $MAPbI_3$ microwires,[37] but are more than those of previously reported $MAPbI_3$ film based devices.[38] In addition, EQE reaches the highest value of 5.32 × 10^2%, which suggests that internal gain plays a significant role in the photoconductive device.

Transient photoresponse of the device to pulsed light of various frequencies from 500 Hz to 10 kHz was recorded on the setup shown in Figure S7a and displayed in Figure S7b−e. According to the relative balance as a function of frequency shown in Figure S7f, the −3 dB bandwidth can be deduced to be about 6.2 kHz, suggesting that the detector can work properly over a wide switching frequency range. A single magnified cycle at a frequency of 6 kHz is then plotted in Figure 3f, from which the response time (τ_r) and recovery time (τ_f) can be extracted to be 52.7 and 57.1 μs, respectively. Significantly, the fast response speed of the photodetector ensures the ability to track rapidly changing optical signals.

Figure 3g and h recorded the channel current of all pixels in an 8 × 8 device unit. Clearly, all the pixels can work properly, and the statistical analysis presents a decent normal distribution curve, giving an average value of 68.8 pA for dark current and 17.1 nA for photocurrent at 3 V bias voltage, respectively. A minor pixel-to-pixel variation exists, and according to our previous research, this may be ascribed to the fluctuation in the thickness of the patterned perovskite films (Figure S8).[25] Due to the difference of the centrifugal force during spin-coating, the pixels closer to the spin axis tend to have a smaller thickness than the farther ones. However, all the pixel devices present an I_{light}/I_{dark} ratio exceed 100 (Figure 3i), enabling the clear distinguishing of the optical signals from the background signals. Meanwhile, the majority of them have an I_{light}/I_{dark} ratio of 200−300, verifying the satisfactory uniformity of the perovskite photodetector arrays and suggesting their potential application in integrated optoelectronic devices.

To realize the real-time imaging of the integrated photodetector arrays, an addressable 8 × 8 perovskite photodetector

https://doi.org/10.1021/acs.jpclett.1c00521
J. Phys. Chem. Lett. 2021, 12, 2930−2936

array was fabricated on the SiO_2/Si substrate with predeposited complex metal circuits (please refer to the Supporting Information for details). As illustrated in Figure S9 and Figure 4c, all pixels share one common electrode, and each pixel has an individual electrode so that each one can work individually without crosstalk. A customized data acquisition system was designed, and the setup is shown in Figures 4a and S10. Specifically, the device was mounted on a lab-built printed circuit board (PCB) and the 64 individual electrodes were connected to four data selections (CD4067) by wire bonding (Au wires, 25 μm in diameter), thus all the device units can be individually addressed by selecting the corresponding input terminal of the data selection (Figure 4b). The channel current of each device unit was acquired in sequence under the control of a single-chip microcomputer (SCM, STC12C5A60S2), which was then converted into a digital signal by the trans-impedance amplifier (TIA, TLC2201) and analog−digital conversion (A/D, STC12C5A60S2). The digital signal was further transmitted to a laptop and self-developed software was then used to perform the image processing. Typically, when a lab-built shadow mask with a hollow "H" pattern (4 mm × 4 mm) was placed between the white light and the photodetector arrays, light penetrating through the hollow region of the mask can be projected on the device units, whereas the rest of the device units were still kept in dark conditions without illumination. The channel currents of all the device units were sequentially acquired and displayed on the screen, giving a well-defined letter "H". The gray scale map of the letter "H" is shown in Figure 4d, where the gray value 255 corresponds to the highest photocurrent upon white light illumination (25 nA) and the gray value 0 corresponds to the dark current of about 77 pA. The real-time imaging system works for 450, 660, and 810 nm light illumination as well and different letters including "F", "U", and "T" can also been clearly displayed (Figure 4d). A video recording the real-time imaging is presented in the Supporting Information (Video S1). Clearly, when we turn on the system upon 660 nm light illumination, the pattern in the mask between the light source and the photodetector arrays (such as a graphic smiley face and a number "3" shown in Figure S11) appears immediately on the screen of the laptop. Limited by the retarding of the readout circuit, the time for imaging is about 1 s, which can be reduced by further circuit optimization. Although the spatial resolution still needs to be further improved by miniaturizing the pixel devices, the integrated photodetector arrays reveal prominent performance in the field of visible light real-time imaging and video capture.

In conclusion, we have demonstrated the uncured PDMS oligomer-assisted patterned fabrication of 8 × 8 addressable perovskite photodetector arrays on periodic hydrophilic/hydrophobic substrates, in which the nanoscale hydrophobic layer is formed by the transferring of small uncured siloxane oligomers from the concaved PDMS stamp to the intimately contacted substrate. The perovskite photodetector arrays present eminent photoresponse characteristics with a responsivity (R) and specific detectivity (D^*) of 2.83 A W^{-1} and 5.4 × 10^{12} Jones upon 660 nm illumination at 3 V bias voltage, respectively, as well as a satisfactory uniformity. Still patterns of "H", "F", "U", and "T" with reasonable resolution have been successfully recorded with a customized data acquisition system, revealing the great potential for real-time visible light image sensing. It is believed that the present method paves the way for the facile, universal, and cost-effective fabrication of addressable photodetector arrays with the potential application in the field of integrated optoelectronic devices, including artificial eyes and wearable devices, due to the good compatibility with solution-based spin-coating processes.

■ ASSOCIATED CONTENT

Supporting Information

The Supporting Information is available free of charge at https://pubs.acs.org/doi/10.1021/acs.jpclett.1c00521.

Details for fabricating the PDMS stamp, patterned growth of perovskite films and fabricating the addressable photodetector arrays, effect of annealing temperature and substrate wettability on the morphology of the perovskite films, SEM images of the patterned $MAPbI_3$ films on different substrates and patterned $FA_{0.85}Cs_{0.15}PbI_3$ films and $MAPbI_{3-x}Cl_x$ films, thickness distribution of the perovskite films, schematic illustration for recording the transient photoresponse of $MAPbI_3$ films PD, schematic illustration of a typical addressable 8 × 8 perovskite photodetector array, photograph of the customized data acquisition system and photographs of the real-time imaging (PDF)

Video recording of the real-time imaging (MP4)

■ AUTHOR INFORMATION

Corresponding Authors

Chun-Yan Wu − *School of Electronic Science and Applied Physics, Hefei University of Technology, Hefei, Anhui 230009, P. R. China;* orcid.org/0000-0001-5793-6772; Email: cywu@hfut.edu.cn

Lin-Bao Luo − *School of Electronic Science and Applied Physics, Hefei University of Technology, Hefei, Anhui 230009, P. R. China;* orcid.org/0000-0001-8651-8764; Email: luolb@hfut.edu.cn

Authors

Bin Wang − *School of Electronic Science and Applied Physics, Hefei University of Technology, Hefei, Anhui 230009, P. R. China*

Chao Zhang − *School of Electronic Science and Applied Physics, Hefei University of Technology, Hefei, Anhui 230009, P. R. China*

Bin Zeng − *School of Electronic Science and Applied Physics, Hefei University of Technology, Hefei, Anhui 230009, P. R. China*

Chao Xie − *School of Electronic Science and Applied Physics, Hefei University of Technology, Hefei, Anhui 230009, P. R. China;* orcid.org/0000-0003-4451-767X

Di Wu − *School of Physics and Microelectronics, Zhengzhou University, Zhengzhou 450052, China;* orcid.org/0000-0003-3266-0612

Yu-Xue Zhou − *College of Physical Science and Technology, Yangzhou University, Yangzhou 225002, China*

Complete contact information is available at: https://pubs.acs.org/10.1021/acs.jpclett.1c00521

Notes

The authors declare no competing financial interest.

■ ACKNOWLEDGMENTS

This work was supported by the National Natural Science Foundation of China (nos. 62074048, 61675062, and

51902078), the Anhui Provincial Natural Science Foundation (2008085MF205), and the Fundamental Research Funds for the Central Universities (PA2020GDKC0014, JZ2020HGTB0051, JZ2018HGXC0001, and JZ2018HGPB0275).

REFERENCES

(1) Wang, H.; Kim, D. H. Perovskite-Based Photodetectors: Materials and Devices. *Chem. Soc. Rev.* **2017**, *46*, 5204−5236.
(2) Lin, Y. H.; Pattanasattayavong, P.; Anthopoulos, T. D. Metal-Halide Perovskite Transistors for Printed Electronics: Challenges and Opportunities. *Adv. Mater.* **2017**, *29*, 1702838.
(3) Teng, F.; Hu, K.; Ouyang, W.; Fang, X. Photoelectric Detectors Based on Inorganic p-Type Semiconductor Materials. *Adv. Mater.* **2018**, *30*, 1706262.
(4) Saparov, B.; Mitzi, D. B. Organic-Inorganic Perovskites: Structural Versatility for Functional Materials Design. *Chem. Rev.* **2016**, *116*, 4558−4596.
(5) Al-Amri, A. M.; Cheng, B.; He, J. H. Perovskite Methylammonium Lead Trihalide Heterostructures: Progress and Challenges. *IEEE Trans. Nanotechnol.* **2019**, *18*, 1−12.
(6) Zhou, J.; Huang, J. Photodetectors Based on Organic-Inorganic Hybrid Lead Halide Perovskites. *Adv. Sci.* **2018**, *5*, 1700256−1700280.
(7) Lee, L.; Baek, J.; Park, K. S.; Lee, Y. E.; Shrestha, N. K.; Sung, M. M. Wafer-Scale Single-Crystal Perovskite Patterned Thin Films Based on Geometrically-Confined Lateral Crystal Growth. *Nat. Commun.* **2017**, *8*, 15882−15890.
(8) Jeong, B.; Han, H.; Park, C. Microand Nanopatterning of Halide Perovskites Where Crystal Engineering for Emerging Photoelectronics Meets Integrated Device Array Technology. *Adv. Mater.* **2020**, *32*, 2000597.
(9) Gao, L.; Zeng, K.; Guo, J.; Ge, C.; Du, J.; Zhao, Y.; Chen, C.; Deng, H.; He, Y.; Song, H.; et al. Passivated Single-Crystalline $CH_3NH_3PbI_3$ Nanowire Photodetector with High Detectivity and Polarization Sensitivity. *Nano Lett.* **2016**, *16*, 7446−7483.
(10) Hassan, Y.; Song, Y.; Pensack, R. D.; Abdelrahman, A. I.; Kobayashi, Y.; Winnik, M. A.; Scholes, G. D. Structure-Tuned Lead Halide Perovskite Nanocrystals. *Adv. Mater.* **2016**, *28*, 566−573.
(11) Gu, L.; Poddar, S.; Lin, Y.; Long, Z.; Zhang, D.; Zhang, Q.; Shu, L.; Qiu, X.; kam, M.; Javey, A.; et al. A Biomimetic Eye with a Hemispherical Perovskite Nanowire Array Retina. *Nature* **2020**, *581*, 278−282.
(12) Song, Y. M.; Xie, Y.; Malyarchuk, V.; Xiao, J.; Jung, I.; Choi, K. J.; Liu, Z.; Park, H.; Lu, C.; Kim, R. H.; et al. Digital Cameras with Designs Inspired by The Arthropod Eye. *Nature* **2013**, *497*, 95−99.
(13) Bao, C.; Yang, J.; Bai, S.; Xu, W.; Yan, Z.; Xu, Q.; Liu, J.; Zhang, W.; Gao, F. High Performance and Stable All-Inorganic Metal Halide Perovskite-Based Photodetectors for Optical Communication Applications. *Adv. Mater.* **2018**, *30*, 1803422.
(14) Jeong, B.; Hwang, I.; Cho, S. H.; Kim, E. H.; Cha, S.; Lee, J.; Kang, H. S.; Cho, S. M.; Choi, H.; Park, C. Solvent-Assisted Gel Printing for Micropatterning Thin Organic-Inorganic Hybrid Perovskite Films. *ACS Nano* **2016**, *10*, 9026−9035.
(15) Wang, S. H.; Jiang, Y.; Juarez-Perez, E. J.; Ono, L. K.; Qi, Y. B. Accelerated Degradation of Methylammonium Lead Iodide Perovskites Induced by Exposure to Iodine Vapour. *Nat. Energy* **2017**, *2*, 16195−16203.
(16) Chou, S. S.; Swartzentruber, B. S.; Janish, M. T.; Meyer, K. C.; Biedermann, L. B.; Okur, S.; Burckel, D. B.; Carter, C. B.; Kaehr, B. Laser Direct Write Synthesis of Lead Halide Perovskites. *J. Phys. Chem. Lett.* **2016**, *7*, 3736−3741.
(17) Alias, M. S.; Dursun, I.; Shi, D.; Saidaminov, M. I.; Diallo, E. M.; Priante, D.; Ng, T. K.; Bakr, O. M.; Ooi, B. S. Focused-Ion Beam Patterning of Organolead Trihalide Perovskite for Subwavelength Grating Nanophotonic Applications. *J. Vac. Sci. Technol., B: Nanotechnol. Microelectron.: Mater., Process., Meas., Phenom.* **2015**, *33*, 051207.
(18) Ashley, M. J.; O'Brien, M. N.; Hedderick, K. R.; Mason, J. A.; Ross, M. B.; Mirkin, C. A. Templated Synthesis of Uniform Perovskite Nanowire Arrays. *J. Am. Chem. Soc.* **2016**, *138*, 10096−10099.
(19) Mao, J.; Sha, W. E.; Zhang, H.; Ren, X.; Zhuang, J.; Roy, V. A.; Wong, K. S.; Choy, W. C. Novel Direct Nanopatterning Approach to Fabricate Periodically Nanostructured Perovskite for Optoelectronic Applications. *Adv. Funct. Mater.* **2017**, *27*, 1606525.
(20) Feng, J.; Jiang, X.; Yan, X.; Wu, Y.; Su, B.; Fu, H.; Yao, J.; Jiang, L. Capillary-Bridge Lithography" for Patterning Organic Crystals toward Mode-Tunable Microlaser Arrays. *Adv. Mater.* **2017**, *29*, 1603652.
(21) Feng, J.; Cheng, G.; Gao, H.; Wen, W.; Gong, Y.; Jiang, X.; Bo, Z.; Wu, Y.; Wu, Y.; Fu, H.; et al. Single-Crystalline Layered Metal-Halide Perovskite Nanowires for Ultrasensitive Photodetectors. *Nat. Electron.* **2018**, *1*, 404−410.
(22) Lee, W.; Lee, J.; Yun, H.; Kim, J.; Park, J.; Choi, C.; Kim, D. C.; Seo, H.; Lee, H.; Yu, J. W.; et al. High-Resolution Spin-on-Patterning of Perovskite Thin Films for a Multiplexed Image Sensor Array. *Adv. Mater.* **2017**, *29*, 1702902.
(23) Wang, G.; Li, D.; Cheng, H.-C.; Li, Y.; Chen, C. Y.; Yin, A.; Zhao, Z.; Lin, Z.; Wu, H.; He, Q.; et al. Wafer-Scale Growth of Large Arrays of Perovskite Microplate Crystals for Functional Electronics and Optoelectronics. *Sci. Adv.* **2015**, *1*, No. e1500613.
(24) Wu, W.; Wang, X.; Han, X.; Yang, Z.; Gao, G.; Zhang, Y.; Hu, J.; Tan, Y.; Pan, A.; Pan, C. Flexible Photodetector Arrays Based on Patterned $CH_3NH_3PbI_{3-x}Cl_x$ Perovskite Film for Real-Time Photosensing and Imaging. *Adv. Mater.* **2019**, *31*, 1805913.
(25) Wu, C. Y.; Wang, Z.; Liang, L.; Gui, T.; Zhong, W.; Du, R.-C.; Xie, C.; Wang, L.; Luo, L. B. Graphene-Assisted Growth of Patterned Perovskite Films for Sensitive Light Detector and Optical Image Sensor Application. *Small* **2019**, *15*, 1900730.
(26) Liu, P.; He, X.; Ren, J.; Liao, Q.; Yao, J.; Fu, H. Organic-Inorganic Hybrid Perovskite Nanowire Laser Arrays. *ACS Nano* **2017**, *11*, 5766−5773.
(27) Kim, T. H.; Cho, K.-S.; Lee, E. K.; Lee, S. J.; Chae, J.; Kim, J. W.; Kim, D. H.; Kwon, J. Y.; Amaratunga, G.; Lee, S. Y.; et al. Full-Colour Quantum Dot Displays Fabricated by Transfer Printing. *Nat. Photonics* **2011**, *5*, 176−182.
(28) Choi, M. K.; Yang, J.; Kang, K.; Kim, D. C.; Choi, C.; Park, C.; Kim, S. J.; Chae, S. I.; Kim, T. H.; Kim, J. H.; et al. Wearable Red-Green-Blue Quantum Dot Light-Emitting Diode Array Using High-Resolution Intaglio Transfer Printing. *Nat. Commun.* **2015**, *6*, 7149.
(29) Kim, J. H.; Hwang, H. S.; Hahm, S. W.; Khang, D. Y. Hydrophobically Recovered and Contact Printed Siloxane Oligomers for General-Purpose Surface Patterning. *Langmuir* **2010**, *26*, 13015−13019.
(30) Xia, Y. N.; Whitesides, G. M. Soft Lithography. *Angew. Chem., Int. Ed.* **1998**, *37*, 550−575.
(31) Li, Y.; Zhang, Y.; Li, T.; Li, M.; Chen, Z.; Li, Q.; Zhao, H.; Sheng, Q.; Shi, W.; Yao, J. Ultrabroadband, Ultraviolet to Terahertz, and High Sensitivity $CH_3NH_3PbI_3$ Perovskite Photodetectors. *Nano Lett.* **2020**, *20*, 5646−5654.
(32) Li, J.; Shen, Y.; Liu, Y.; Shi, F.; Ren, X.; Niu, T.; Zhao, K.; Liu, S. F. Stable High-Performance Flexible Photodetector Based on Upconversion Nanoparticles/Perovskite Microarrays Composite. *ACS Appl. Mater. Interfaces* **2017**, *9*, 19176−19183.
(33) Jansen-van Vuuren, R. D.; Armin, A.; Pandey, A. K.; Burn, P. L.; Meredith, P. Image and Signal Sensors for Computing and Machine Vision: Developments to Meet Future Needs. *Adv. Mater.* **2016**, *28*, 4766.
(34) Dou, L.; Yang, Y.; You, J.; Hong, Z.; Chang, W. H.; Li, G.; Yang, Y. Solution-Processed Hybrid Perovskite Photodetectors with High Detectivity. *Nat. Commun.* **2014**, *5*, 5404.
(35) Baeg, K. J.; Binda, M.; Natali, D.; Caironi, M.; Noh, Y. Y. Organic Light Detectors: Photodiodes and Phototransistors. *Adv. Mater.* **2013**, *25*, 4267−4295.
(36) Yang, C.; El-Demellawi, J.; Yin, K. J.; Velusamy, D. B.; Emwas, A. H. M.; El-Zohry, A. M.; Gereige, I.; AlSaggaf, A.; Bakr, O. M.; Alshareef, H. N.; et al. $MAPbI_3$ Single Crystals Free from Hole-

https://doi.org/10.1021/acs.jpclett.1c00521
J. Phys. Chem. Lett. 2021, 12, 2930−2936

Trapping Centers for Enhanced Photodetectivity. *ACS Energy Lett.* **2019**, *4*, 2579−2584.
(37) Deng, W.; Zhang, X.; Huang, L.; Xu, X.; Wang, L.; Wang, J.; Shang, Q.; Lee, S. T.; Jie, J. Aligned Single-Crystalline Perovskite Microwire Arrays for High-Performance Flexible Image Sensors with Long-Term Stability. *Adv. Mater.* **2016**, *28*, 2201−2208.
(38) Hu, X.; Zhang, X.; Liang, L.; Bao, J.; Li, S.; Yang, W.; Xie, Y. High-Performance Flexible Broadband Photodetector Based on Organolead Halide Perovskite. *Adv. Funct. Mater.* **2014**, *24*, 7373−7380.

https://doi.org/10.1021/acs.jpclett.1c00521
J. Phys. Chem. Lett. 2021, 12, 2930−2936